Interpretation of high-order commensurate phases for an argon monolayer adsorbed on Pt(111)

C. Ramseyer, P. N. M. Hoang, and C. Girardet
Laboratoire de Physique Moléculaire, Université de Franche Comté, 25030 Besançon Cedex, France
(Received 12 February 1993)

Recent helium atom scattering experiments have shown that Ar monolayers form high-order commensurate (HOC) phases on Pt(111) substrate at low temperature and that HOC-HOC transitions proceed as functions of coverage and temperature. This leads to the realization of a two-dimensional devil's staircase. Potential calculations using effective pairwise Pt-Ar and Ar-Ar interactions and substrate-mediated Ar-Ar/Pt contributions are performed to determine the equilibrium geometries of the monolayer vs Ar coverage. The free energy calculated at finite temperature ($T \leq 50$ K) shows that five metastable hexagonal HOC structures occur within the range $31 \leq T \leq 46$ K. When T increases in this range, the nonrotated structures appear with increasing lattice parameters 3.71, 3.78, 3.82, 3.84, and 3.89 Å. The most stable geometry is a (4×4) unit cell with 9 Ar atoms. Rotated phases exhibit the same behavior with, however, a slightly shifted temperature range and shifted values for the lattice parameter. These results are in close agreement with the experimental findings and they corroborate the devil's staircase event for such a system.

I. INTRODUCTION

Much experimental and theoretical[1–5] effort has been devoted to the determination of monolayer geometries of adsorbates on various substrates, and to the analysis of commensurate-to-commensurate, or commensurate-to-incommensurate phase transitions as functions of coverage and temperature. High-order commensurate (HOC) structures characterized by relatively large unit cells containing several atoms are observed either for metal and molecule adsorbates on metal substrate systems,[3,5–7] or for rare-gas atoms and small molecules adsorbed on corrugated substrates[8–10] such as graphite and MgO. By using thermal helium atom elastic scattering, the Jülich group[3] has recently explored[3,11] the structure of rare-gas layers (Ar, Kr, Xe) physisorbed on clean Pt(111) in the submonolayer coverage regime. The existence of HOC hexagonal phases and of incommensurate/HOC transition for krypton atoms adsorbed on Pt(111) has been evidenced clearly. For argon, first-order HOC/HOC phase transitions are observed with a stepwise variation of the lattice parameter in the primitive cells characterizing a devil's staircase behavior. A detailed analysis of the phase diagram for this latter system exhibits the following features.[11]

(i) At $T = 25$ K, there is a phase transition from a hexagonal structure with lattice parameter $a_M = 3.81$ Å to a structure in which $a_M = 3.70$ Å. These structures correspond to a coverage below and above 0.75 monolayer (ML), respectively.

(ii) The high coverage phase, stable below 33 K is HOC with a (4×4) nonrotated structure containing nine argon atoms per primitive cell, and a lattice spacing equal to 3.70 Å.

(iii) The low coverage phase has lattice parameters equal to either 3.81 or 3.83 Å depending on the time and annealing temperature; the thermal expansion is clearly irreversible.

(iv) The coverage regime largely depends on the preparation of the adlayer, since the compressed phase is already observed at low temperature for low coverage 0.4 ML, but it changes into an expanded one by annealing at 35 K when the overall coverage is smaller than 0.7 ML.

(v) Discontinuous transitions and partially locked phase coexistence are obtained at the low coverage regime with a discrete increase of the lattice parameters 3.81, 3.84, and 3.88 Å.

The aim of the present paper is to interpret these features on the basis of potential calculations. Simple forms of interaction potentials for the adsorbate-substrate system are available, which can reproduce some experimental data for a single Ar adatom. The influence of the lateral interactions is taken into account both through Ar-Ar pairwise contributions and by considering substrate-mediated potentials. The total interaction potential is minimized with respect to the position of the argon atoms for selected HOC geometries containing an increasing number of atoms. The calculation of the monolayer dynamics, within the rigid substrate approximation, allows us to determine the free energy per atom for every HOC structure and to compare the relative stability of these geometries. We present the interaction potentials in Sec. II, and the minimization procedure and the free energy calculation in Sec. III. The numerical results are compared to experimental data in Sec. IV.

II. INTERACTION POTENTIAL

The triangular Pt(111) surface with lattice parameter $a_s = 2.78$ Å is assumed to be ideal and rigid. The Ar

 ©1994 The American Physical Society

monolayer is hexagonal with a variable lattice parameter a_M depending on the coverage. Furthermore the layer, as a whole, can rotate in a plane parallel to the surface, as shown below (Fig. 1). The interaction potential V is a sum of an intralayer contribution V_M and an adsorbate-substrate term V_{MS}. V_M is described by a pairwise Lennard-Jones potential

$$V_M = \sum_{l,s} \sum_{l',s'} \sum_{k=6,12} (-1)^{k/2} \frac{C_k}{r\binom{l\ l'}{s\ s'}^k}, \quad (1)$$

where $r\binom{l\ l'}{s\ s'}$ defines the distance between the sth and s'th argon atoms pertaining, respectively, to the lth and l'th unit cells. The unit cell characterizing the order of commensurability of the admonolayer must be defined for each HOC phase. The monolayer-substrate potential V_{MS} is described by an effective atom-atom Lennard-Jones potential with two empirical parameters and by a substrate-mediated contribution with two calculated parameters, as[12]

$$V_{MS} = \sum_{l,s} \sum_{m,p} \sum_{k=6,12} (-1)^{k/2} \frac{C_k}{r\binom{l\ m}{s\ p}^k} + \frac{1}{2} \sum_{l,s} \sum_{l',s'} \left\{ \frac{4}{3} \frac{C_1}{r\binom{l\ l'}{s\ s'}^3} \left[\frac{\left[\bar{z}\binom{l\ l'}{s\ s'}^2 + r\binom{l\ l'}{s\ s'}^2\right]^2}{\left[4\bar{z}\binom{l\ l'}{s\ s'}^2 + r\binom{l\ l'}{s\ s'}^2\right]^{\frac{5}{2}}} \right] - \frac{C_2}{\left[4\bar{z}\binom{l\ l'}{s\ s'}^2 + r\binom{l\ l'}{s\ s'}^2\right]^3} \right\}. \quad (2)$$

$r\binom{l\ m}{s\ p}$ defines the distance between the (l,s)th monolayer atom and the mth Pt atom belonging to the pth substrate plane ($p = 0$ is the surface plane) ; $\bar{z}\binom{l\ l'}{s\ s'}$ is the arithmetic average of the distance between the (l,s)th and (l',s')th pair Ar atoms and the surface. Note that the substrate-mediated contributions C_1 and C_2 have already been summed over the whole substrate. Though smaller than the pairwise contribution, this latter interaction cannot be disregarded in the calculation of the equilibrium structures, as shown elsewhere[12] for metal substrates. The parameters C_k ($k = 1, 2, 6, 12$) are given in Table I.

Figure 2 displays the behavior of the potential V_{MS} for an Ar atom adsorbed on Pt(111) as functions of the atom-surface distance z. The potential curves labeled (1) and (1′) are drawn for two characteristic sites : the hollow site (1) where the Ar atom lies at the center of the regular triangle formed by three nearest-neighbor Pt atoms, and the on-top site (1′), i.e., above a Pt atom. The hollow site appears to be more stable by about 10% than the on-top site, with a corresponding distance $z = 3.22$ Å instead of 3.40 Å. Such a potential accurately fits two experimental data:[3] the adsorption energy at 0 K equal to 80 meV for the single adatom, and the vibrational adbond frequency equal to 5 meV.

In Fig. 2 we give the behavior of other interaction potentials proposed in the literature, which are in general fitted to experimental desorption and scattering data. Curve (2) corresponds[13] to a Morse potential which fits well the well depth, but leads to values of the vibrational frequency twice that of the experimental data.[14] The potential connected to curve (3) has a Lennard-Jones form with an additional cutoff contribution which gives[15] a reasonable, though too small, frequency, but has an erroneous potential depth. Curve (4), also built from a Lennard-Jones contribution, takes into account the electronic distribution at the metal surface through an additional term;[16] the frequency obtained agrees with the

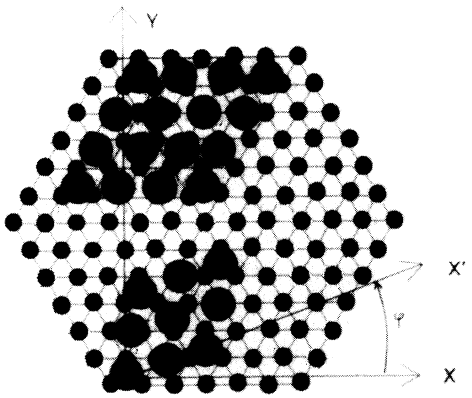

FIG. 1. Geometry of the Pt(111) substrate (dark small circles represent Pt atoms) with two adlayer HOC structures (hatched large circles represent Ar atoms). Lower: rotated (2×2) geometry, $m_1 = 2$ along **X** and $m_2 = 1$ along **Y**; upper: nonrotated (4×4) geometry, $m_1 = 4$ along **X**, and $m_2 = 0$ along **Y**.

TABLE I. Potential parameters. The C_6 and C_{12} parameters for the Ar-Pt pair are estimated from data given in Refs. 11 and 14; the corresponding Lennard-Jones parameters ϵ and σ for Pt are $\sigma = 3.37$ Å and $\epsilon = 6.6$ meV. The substrate-mediated coefficients C_1 and C_2 are calculated from Ref. 12 and data in Ref. 21.

	C_6 (eV Å^6)	C_{12} (eV Å^{12})	C_1 (eV Å^6)	C_2 (ev Å^{12})
Ar-Ar	67.45	$9.25\ 10^4$	-	-
Ar-Pt	51.45	$7.27\ 10^4$	24.62	17.32

experimental value, but the potential depth seems too large by about 20%. This latter potential, which appears to be realistic, could be used here, but it is relatively complicated in the sense that six parameters must be determined whereas only two are required for the potential labeled (1). Note the dispersion of the potential curves, indicating the poor knowledge of parameters for such systems. This is particularly striking for the atom-surface distance, which fluctuates from 2.8 to 4.1 Å.

III. THEORETICAL BACKGROUNDS

A. Numerical minimization procedure

The determination of the equilibrium monolayer geometries is done according to a method which is close to the Novaco-MacTague approach,[17] devoted to incommensurate adsorbed phases, and to the approach by Fuselier, Raich, and Gillis,[18] who calculated the geometry of commensurate argon monolayers adsorbed on graphite. The total interaction potential V is expanded with respect to initial positions of the Ar atoms. These positions are defined by the two-dimensional (2D) triangular arrangement of Pt(111) with a lattice parameter a_M, and with respect to an absolute frame tied to the substrate in which the origin is assumed to be a hollow site. Within this latter assumption, we disregard the eventual shifting of the center of mass of the unit cell, depending on the geometry of this cell. Let $\eta\binom{l}{s}$ be the small displacement of the (l,s)th Ar atom with respect to its initial position $\mathbf{R}\binom{l}{s}$; the assumption of small displacement is valid when a_M does not change by more than 10 % around the value of the lattice parameter $a_F = 3.85$ Å of the hexagonal floating monolayer.[19] We limit the η expansion to the quadratic order. The minimum condition is obtained when[20]

$$\eta_\alpha\binom{l}{s} = \sum_{\beta,l',s'} A^{-1}_{\alpha\beta}\binom{l\ l'}{s\ s'} B_\beta\binom{l'}{s'}, \tag{3}$$

where B and A, respectively, characterize the first and second derivatives of the V potential with respect to η, which are connected to the force and force constant on the (l,s)th atom. Without additional requirements, the system of Eq. (3) is infinite, or at least very large, as expected in practice for an incommensurate structure. However, when we consider commensurate phases, periodic conditions are applied to η in order to reduce in a drastic way the number of atoms, namely those contained in a primitive cell $l = 0$. The size of the primitive cell and its orientation φ with respect to the substrate are then varied. This orientation is characterized by a rotation of angle φ $(0 \le \varphi \le \frac{\pi}{6})$ around the previously defined origin (hollow site), as shown in Fig. 1. Due to symmetry, larger values of φ give redundant structures. We determine all possible high-order commensurate geometries, with primitive translation vectors $\mathbf{a}_{M_1}$ and $\mathbf{a}_{M_2}$ obeying the conditions

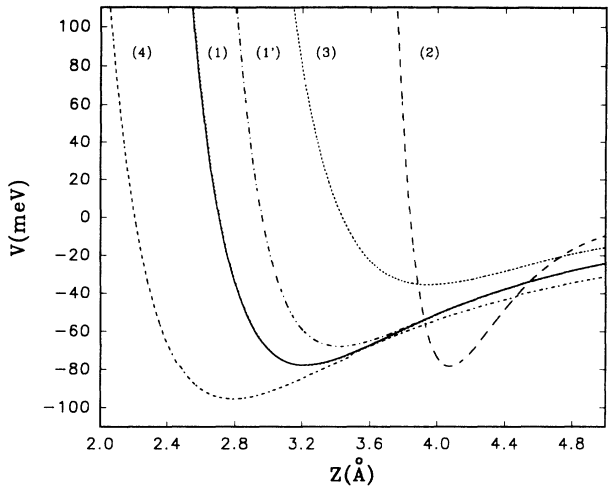

FIG. 2. Interaction potentials V (meV) for an Ar atom adsorbed on Pt(111) vs the atom-surface distance z; (1) and (1′) Lennard-Jones form with the Ar atom on a hollow or on-top site, respectively; (2) Morse potential; (3) and (4) Lennard-Jones form with additional contributions (see text).

$$\begin{aligned} &|\,\mathbf{a}_{M_1}\,| = |\,\mathbf{a}_{M_2}\,|, \\ &(\mathbf{a}_{M_1}, \mathbf{a}_{M_2}) = \frac{\pi}{3}. \end{aligned} \tag{4}$$

That means that we consider all unit cells to have a lozenge shape. Even within this restriction, the number of structures to be calculated is tremendous, and we furthermore limit, in practice, the maximum number of atoms per cell to 256. The registry condition for the HOC geometries leads then to the requirements

$$\begin{aligned} &\frac{a_M}{a_S} = (m_1^2 + m_2^2 + m_1 m_2)^{\frac{1}{2}}/n, \\ &\tan\varphi = \frac{m_2\sqrt{3}}{(2m_1 + m_2)}, \end{aligned} \tag{5}$$

where the set $m = (m_1, m_2)$ of integer numbers defines the position of a Pt atom in the surface plane (Fig. 1):

$$\mathbf{R}\binom{m}{0} = \left(m_1 + \frac{m_2}{2} - \frac{1}{2}\right) a_S\mathbf{X} + (m_2 - 1)a_S\frac{\sqrt{3}}{2}\mathbf{Y}, \tag{6}$$

and the integer number n characterizes the position of the Ar atom at the extremity of the side of the primitive cell:

$$\mathbf{R}\binom{n}{0} = na_M(\cos\varphi\mathbf{X} + \sin\varphi\mathbf{Y}). \tag{7}$$

Note that we take n instead of (n_1, n_2) to satisfy Eq. (5). The ratio a_M/a_S (a_S = const) is varied by 5% around the value 1.354 to take into account the possible registry misfit; this leads to a_M values ranging between 3.6 and 3.9 Å. All the structures defined by m_1, m_2, and n and obeying Eqs. (4) and (5) are minimized with respect to

the positions $\eta\binom{l}{s}$ [Eq. (3)]. The value $\varphi = 0$ ($a_M/a_S = m_1/n$) corresponds to nonrotated structures.

B. HOC phase free energy

The free energy F for every HOC geometry determined above is calculated within the harmonic monolayer approximation by solving the dynamical matrix. This calculation ignores the monolayer-substrate dynamical coupling that may be not negligible at small wave-number values for the vertical mode of the layer. In practice, it can be shown that the Ar atom motions perpendicular to the surface can be separated from the parallel ones, owing to the very weak dispersion of the perpendicular vibrational mode.[14] The perpendicular block of the dynamical matrix is thus a square $N \times N$ matrix, where N is the number of atoms per unit cell of a HOC structure characterized by a coverage θ; the eigenfrequencies $\omega_s(\theta)$ for $s = 1, \ldots, N$ depend on the coverage. For the parallel motions, we take advantage of the fact that our calculations show only small parallel displacements in the determination of the monolayer equilibrium. We therefore assume that the corresponding dynamical matrix with rank $2N$ can be approximated by that of a Debye 2D crystal with a Debye temperature depending on the coverage $T_D(\theta)$ connected to the HOC structure.

The free energy per adatom at temperature T and coverage θ is then written[9]

$$F(T,\theta) = \frac{V(\theta)}{N} + \frac{kT}{N}\sum_{s=1}^{N} \ln\left[2\sinh\left(\frac{\hbar\omega_s(\theta)}{2kT}\right)\right] + \tfrac{2}{3}kT_D(\theta)\left[1 + 6\frac{T}{T_D(\theta)}\xi(\theta,T)\right]. \quad (8)$$

V/N characterizes the minimum potential energy for a HOC cell with N atoms and coverage θ, and ξ defines the function

$$\xi(\theta,T) = \int_0^{T_D(\theta)/T} x\ln[1-\exp(-x)]dx, \quad (9)$$

which appears in the Debye crystal after summing over the vibrational spectrum of the parallel modes.

The coverage dependence of F is thus contained in $V(\theta)$, $w_s(\theta)$, and $T_D(\theta)$. The first two dependencies are accurately determined from the calculations, whereas the third function $T_D(\theta)$ can approximately be estimated by using results on the floating incommensurate 2D Ar monolayer. The Debye temperature T_I and the Grüneisen factor γ_I have been calculated[19] for this structure corresponding to a coverage $\theta_I = 0.515$. For small variations of θ around θ_I, we can assume a linear behavior of T_D as

$$T_D(\theta) = T_I\left(1 - \gamma_I\frac{\theta-\theta_I}{\theta_I}\right), \quad (10)$$

where $T_I = 68$ K, and $\gamma_I = 5.41$. The curves $F(T,\theta)$ can then be drawn using Eq. (8) and this θ dependence of T_D.

IV. NUMERICAL RESULTS AND DISCUSSION

The displacements η of the N atoms in the primitive cell for every HOC structure have been calculated using Eq. (3). The values of the parallel components of $\eta\binom{l}{s}$ are less than 0.5–1 % of the mean lattice constant defined by the ideal hexagonal structure. This indicates that the substrate appears relatively flat to the Ar layer, as shown in Fig. 3. This latter figure displays the potential-energy surface as viewed by an Ar atom adsorbed on Pt(111). The hollow site is the most stable, whereas the on-top Pt site is a maximum, and the energy difference defining the overall corrugation does not reach 10 meV. Moreover, the equilibrium valleys along the medians of the regular triangles are nearly flat (less than 2 meV between the

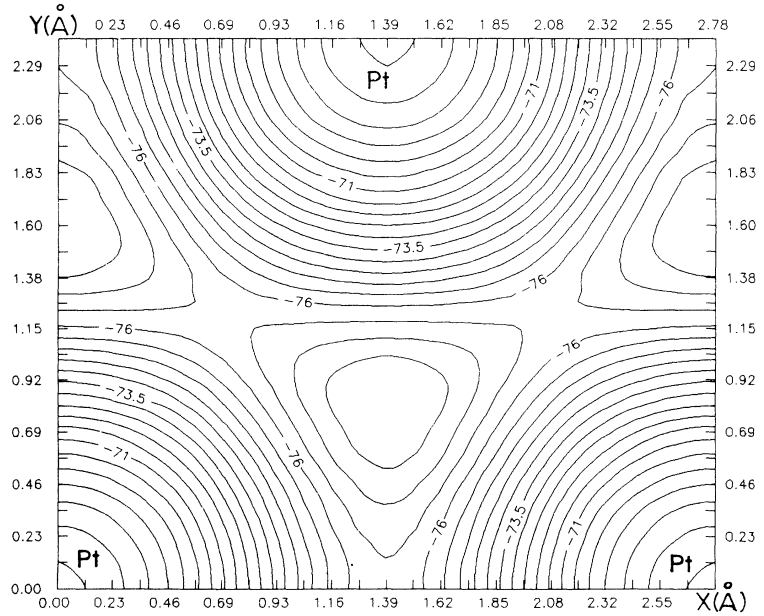

FIG. 3. $(\mathbf{X},\mathbf{Y})$ potential-energy surface V (meV) for an Ar atom adsorbed on Pt(111).

maximum and the minimum). The lateral Ar-Ar potential is also relatively flat over a small range of interatomic distances around the equilibrium distance. Therefore the minimum energy calculated for each HOC geometry is a subtle phenomenon resulting from the competition between the Ar-Ar potential which slightly varies with the coverage, and the adsorbate-substrate potential which depends mainly on the Ar-surface distance through the various sites of the HOC primitive cell (cf. Table II).

As displayed in Fig. 4, the most stable structures, at 0 K, are calculated for a lattice parameter a_M approximately equal to 3.71 Å ($\theta \sim 0.562$). The rotated and nonrotated HOC phases as defined in Fig. 1 fall on the same curve, and the corresponding potential minimum per adatom including the lateral interactions is equal to about −115 meV which can be compared to the experimental[3] value of −97 meV. The mean atom-surface distance is $\bar{z}_M = 3.30$ Å with a standard deviation $\sigma_{z_M} = 0.05$ Å. The corresponding mean value of the adbond vibrational frequency is $\bar{\omega}_\perp = 5.1$ meV, with a standard deviation $\sigma_{\omega_\perp} = 0.09$ meV. Note that the mean distance $\bar{z}_M$ and frequency $\bar{\omega}_\perp$ have identical values for all HOC structures. The most stable structure is the (4×4) hexagonal HOC phase with a lattice parameter $a_M = 3.7$ Å, and a potential energy −115.8 meV (Table II), but it can be mentioned that the energies of all the HOC phases are within a range of about 7 meV at $T = 0$ K.

Figure 5 displays the behavior of the free energy per adatom of the various nonrotated HOC phases as a function of temperature. The influence of $T \leq 50$ K on the value of the free energy with respect to V/N remains small ($\leq 5\%$), but we clearly see the decrease of F when T increases and, more specially, the different slopes of the HOC phases. These slopes are directly connected to the assumed dependence of T_D in Eq. (10), and thus to the value of γ_I. Around 30–35 K, HOC geometries

TABLE II. Comparison of the minimum potential values for various nonrotated HOC structures (at $T = 0$ K).

n	a_M (Å)	θ	V_M (meV)	V_{MS} (meV)	$V_M + V_{MS}$ (meV)
4	3.70	0.562	−42.0	−73.8	−115.8
7	3.89	0.510	−38.8	−74.1	−112.9
11	3.82	0.530	−40.4	−73.9	−114.3
13	3.61	0.591	−40.5	−74.0	−114.5
15	3.79	0.537	−40.9	−74.0	−114.9
17	3.63	0.585	−41.0	−74.0	−115.0
18	3.84	0.520	−39.8	−74.1	−113.9
19	3.77	0.543	−41.1	−74.0	−115.1
21	3.64	0.580	−41.2	−73.9	−115.1

which were not the most stable at 0 K have free-energy curves which intersect the most stable one. In Fig. 6(a), we give an enlargement of the $F(T)$ curves within the range 26–50 K which shows five regions for the nonrotated structures, below 31 K, between 31 and 36 K, between 36 and 42 K, between 42 and 46 K, and above 46 K. The rotated geometries [Fig. 7(a)] behave similarly, with transition temperatures at 34, 37, 42, and 47 K from a metastable geometry to another. In Figs. 6(b) and 7(b) we present the corresponding behavior of F as functions of the coverage for a sampling of temperature ranging between 26 and 50 K, and using a step of 2 K. The full curves with steps exhibit more clearly the occurrence of the successive phases.

For a direct comparison with thermal helium atom scattering data,[11] in Fig. 8 we give the behavior of the lattice parameter a_M for the various HOC nonrotated and rotated structures as functions of the temperature in the range 26–50 K. A striking discrete stepwise behavior is shown with five significant a_M values at 3.71, 3.79, 3.82, 3.84, and 3.89 Å corresponding to the nonrotated structures n=4, 15, 11, 18, and 7, respectively.

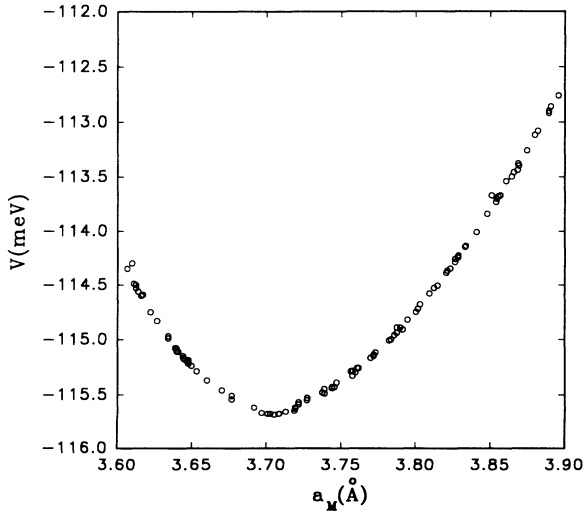

FIG. 4. Potential energy V (meV) as a function of interatomic layer distance a_M (Å) for all HOC structures with less than 256 atoms per primitive cell.

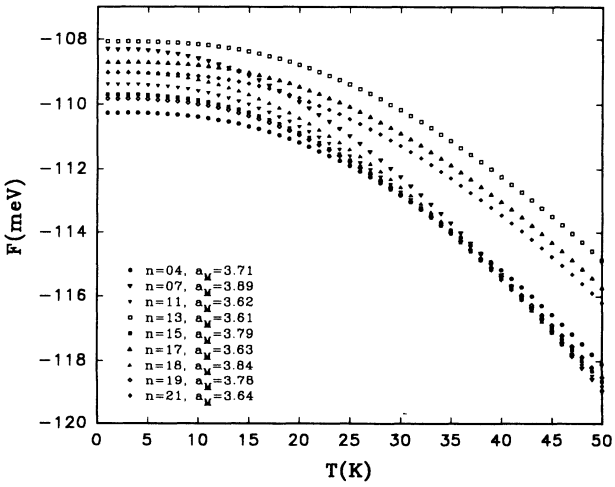

FIG. 5. Free-energy curves F (meV) as a function of temperature T for nonrotated HOC structures. The symbols represent $(n \times n)$ phases with various cell parameters a_M (Å).

Such a result is in good agreement with the experimental findings exhibiting a_M stairs for the values 3.69 and 3.88 Å, and intermediate steps for 3.81, 3.83, and 3.84 Å. All the present features are also in agreement with the qualitative analysis of Zeppenfeld *et al.*,[11] which is based only on geometrical arguments. Their assignment of the more stable structures (n=4, 11, 18, and 7) is close to our results.

The rotated geometries exhibit a similar discrete behavior for $a_M(T)$, though with shifted values for the transition temperatures ($34 \leq T \leq 47$ K) and for the corresponding lattice parameters (a_M=3.72, 3.79, 3.82, 3.87, and 3.90 Å). Some of these structures are nearly as stable

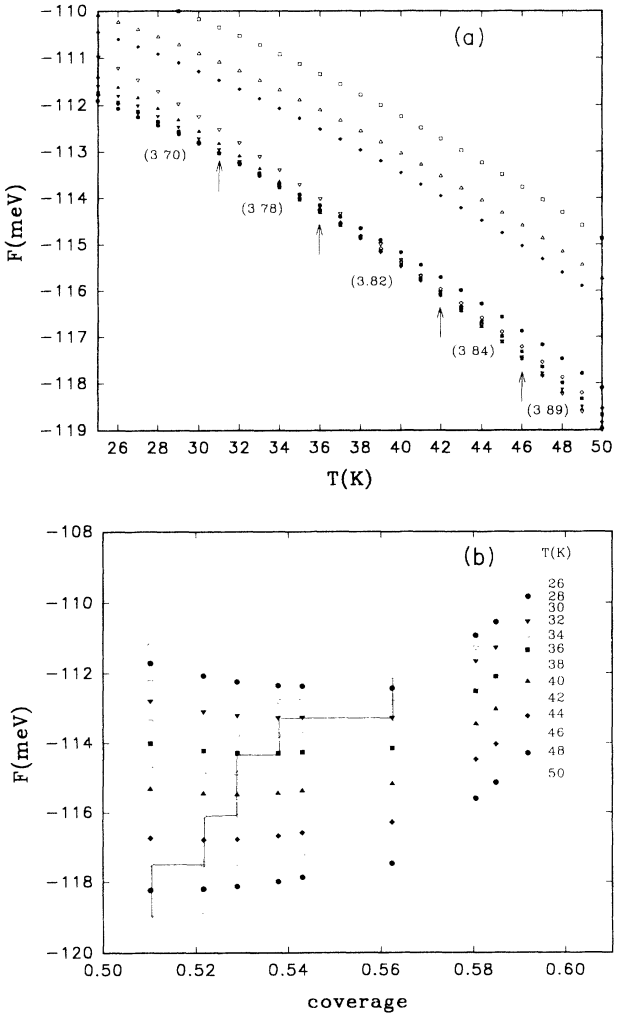

FIG. 6. (a) Free energy F (meV) for the nonrotated structures in the temperature range leading to phase transitions. Same symbols as in Fig. 5. The arrows show the phase transitions. (b) Free energy F (meV) vs coverage θ. Symbols refer to various temperatures ranging between 26 and 50 K, with a step of 2 K. The transitions are indicated by the full curve. Note that the double tangent construction should in fact strictly be done in the free energy per particle F as a function of the inverse number density (coverage), in order to maintain the chemical potential and pressure of two phases in equilibrium.

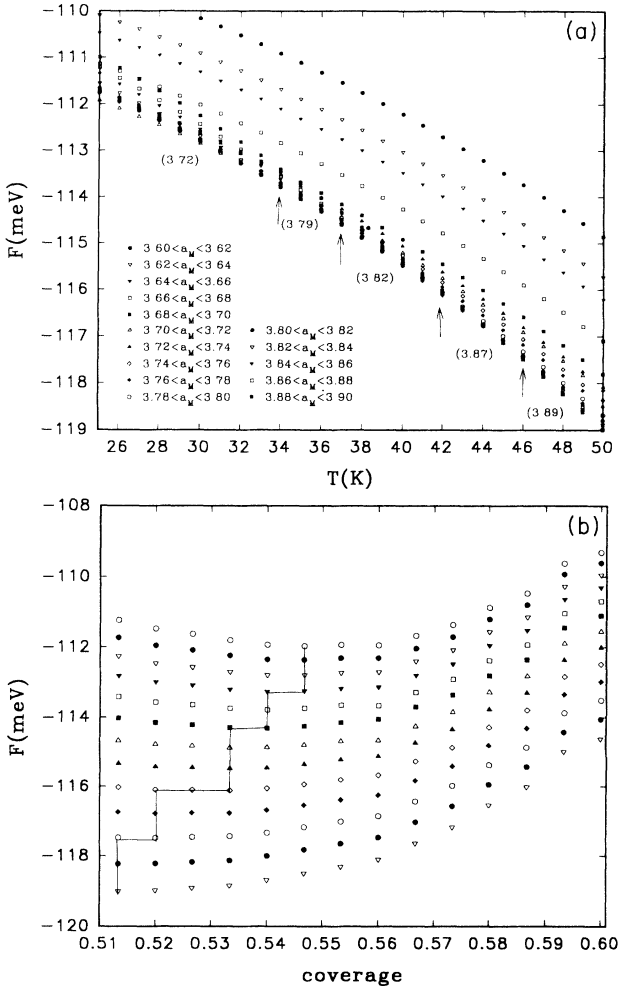

FIG. 7. (a) Free energy F (meV) for the rotated structures in the temperature range leading to the phase transitions. Symbols refer to lattice parameter ranges for the HOC structures. (b) Free energy F (meV) as a function of coverage θ; see caption to Fig. 6(b). The transitions are indicated by the full curve.

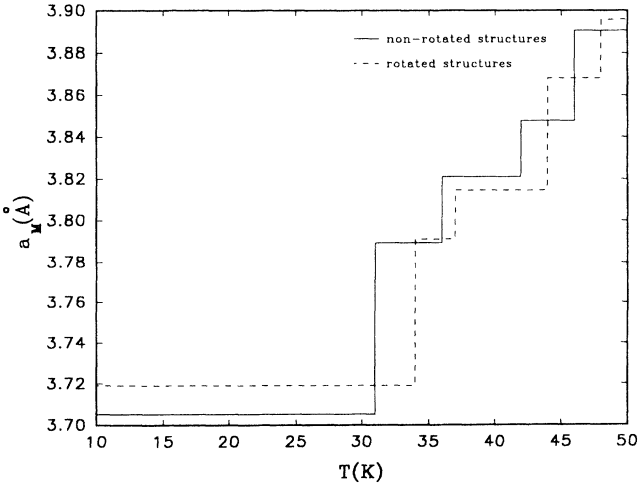

FIG. 8. Behavior of the lattice parameter a_M (Å) for the nonrotated (full curve) and rotated (broken curve) HOC structures vs temperature exhibiting a devil's staircase.

as nonrotated structures. It is difficult to explain, from the present results, why nonrotated HOC phases seem to occur preferentially in experiments. In Fig. 9, we calculate the number of HOC phases which occur at a coverage $\theta \pm \Delta\theta/2$ with $\Delta\theta = 0.003$, in the range $0.5 \leq \theta \leq 0.6$, whatever angle φ. On this histogram, which appears to be relatively regular, we also show the ranges containing nonrotated HOC structures. These structures are generally located in boxes with maximum height, indicating a high density of rotated structures with the same coverage. We can thus conclude that angle φ is not a severe criterion for the calculation of the structure stability. As a consequence, an interpretation of the occurrence of mainly nonrotated phases is probably due to another mechanism. This can be due, for instance, to the existence of steps on the Pt(111) surface, which could favor domains along directions which correspond to diffusion valleys along $\mathbf{X}$ and along $\mathbf{Y}'$ rotated by $\frac{\pi}{6}$ with respect to $\mathbf{X}$. Such valleys are clearly equilibrium channels which are very flat for the Ar atoms, as shown in Fig. 3. Such a hypothesis is in fact corroborated by experiments which show[22] the occurrence of rotated Ar and Kr phases after a preliminary adsorption of a mobile adsorbate on the substrate steps. Thus an $R30°$ geometry is clearly observed for an Ar monolayer when a small amount of Kr atoms is preadsorbed on Pt(111). Experiments also indicate[23] that nonrotated and $R30°$ structures are stable on Pt(111) without transition from one to another, although their adsorption energies are probably very close. It would be interesting to determine the activation energy required for the transition from the nonrotated to the $R30°$ phase.

It should be mentioned that the energies of all the HOC geometries considered lie in a range less than 10 meV. This value represents about 6% of the total interaction potential per adatom between the monolayer and the substrate. Due to the present potential accuracy, such an agreement between experiments and calculations can be fortuitous, but such a striking consistency in the occurrence of devil's staircase transitions tends to demonstrate that the present model, though very simple, looks accurate.

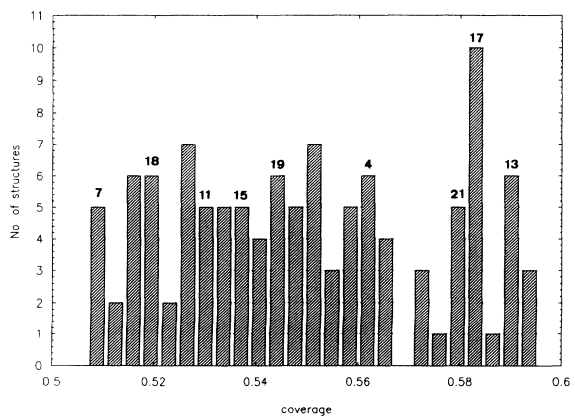

FIG. 9. Histogram of the HOC structures as a function of the layer coverage. Each box with an upper number contains the corresponding $(n \times n)$ nonrotated structure.

It is interesting to compare our approach with that of Ref. 18. In their paper,[18] Fuselier, Raich, and Gillis determine the equilibrium orientations and lattice constants of commensurate Ar monolayers adsorbed on the basal plane of graphite, by minimizing the free energy F of the layer-substrate system. Within the quasiharmonic approximation for the layer dynamics, this free energy appears to be the sum of three main terms: the floating monolayer contribution, the lock-in terms due to the substrate corrugation without monolayer distortion, and the contribution provided by the monolayer distortion as defined by Novaco and McTague.[17] When the third term in F is disregarded, the relationship between angle φ and lattice parameter a_M is determined by geometric considerations which look like those given by Eq. (5), changing the substrate spacing and corrugation. The stable commensurate structures in the (φ, a_M) plane are then calculated, by assuming a structureless substrate for the monolayer dynamics, with a mean perpendicular mode frequency $\bar{\omega}_\perp$ equal to 5.3 meV, and an average energy of about -82 meV. It is shown that the lowest energies are obtained for small coincident cells containing few argon atoms and rotated by a few degrees, but all the HOC structures considered have energy values ranging within 0.2 meV, around the average energy of the incommensurate structure. The fact that, on the one hand, the monolayer distortion term is considered only at $T = 0$ K and, on the other hand, the monolayer-substrate potential associated with the monolayer dynamics is restricted to the lowest-order Fourier amplitudes in the calculation of the third contribution (Novaco-McTague term), can be responsible for inaccuracies and does not allow the authors of Ref. 18 to determine the relative stability of commensurate and incommensurate phases at finite temperature. Indeed, such a truncation of the potential expansion results in an improper favoring of the HOC phase against the incommensurate phase. In our approach, such inaccuracies do not exist, since we use a direct sum technique. It has been verified that the truncation in this direct sum procedure does not influence the results. We show that the energy sequency range for the occurrence of stable commensurate structures is larger. This is the major difference between the graphite and platinum substrates, the second leading to the lock-in of HOC Ar phases.

V. CONCLUSION

The series of HOC phases which have been observed[11] in the physisorption of Ar on Pt(111) can be explained fairly well on the basis of simple interaction potentials including substrate-mediated contributions. In particular, the observed phase transitions leading to an incomplete devil's staircase can be interpreted adequately both on the basis of a very subtle competition between the intralayer and layer-substrate interactions, and that of additional contributions arising from the temperature and coverage variations of the layer dynamics. These variations can mainly be taken into account through the dependence of the Debye temperature as a function of the coverage. The free energies of most HOC structures

lie within a narrow range, indicating the possibility of easy transitions from one to another when temperature and/or coverage are slightly changed. In this sense, the Ar monolayer on Pt(111) is a model system for testing interaction potential accuracy through the behavior of phase transitions. Similar calculations for the heaviest rare-gas monolayers could be performed within the same approach, for example to study the coexistence of incommensurate and HOC phases for Kr and N_2 adsorbed on Pt(111),[8] and for Xe adsorbed on Cu(110).[23]

ACKNOWLEDGMENTS

The authors wish to acknowledge Dr. P. Zeppenfeld (KFA-Forschungszentrum Jülich. D) for very stimulating and fruitful discussions and for improving the text. The Laboratoire de Physique Moléculaire is "Unité Associée au Centre National de la Recherche Scientifique No. 772."

[1]J.G. Dash and J. Ruvalds, in *Phase Transition in Surface Films* (Plenum, New York, 1980).
[2]S.K. Shina, in *Ordering in Two Dimensions* (Elsevier, New York, 1980).
[3]K. Kern and G. Comsa, in *Phase transitions in Surface Films 2*, edited by H. Taub *et al.* (Plenum, New York, 1991), p. 41, and references quoted therein; K. Kern, P. Zeppenfeld, R. David, and G. Comsa, Phys. Rev. B **35**, 886 (1987).
[4]P. Bak, Rep. Prog. Phys. **45**, 587 (1982).
[5]B.N.J. Person, Surf. Sci. Rep. **15**, 1 (1992), and references quoted therein.
[6]P. Feuter and T. Gustafsson, Phys. Rev. B **43**, 195 (1991).
[7]K.S. Liang, K.L. D'Amico, C.H. Lee, and E.Y. Shen, Phys. Rev. Lett. **65**, 3025 (1990).
[8]K. Kern, P. Zeppenfeld, R. David, and G. Comsa, Phys. Rev. Lett. **59**, 79 (1987).
[9]T. Meichel, J. Suzanne, C. Girard, and C. Girardet, Phys. Rev. B **38**, 3781 (1988).
[10]H. Freimuth, H. Wiechert, H.P. Schildberg, and H.J. Lauter, Phys. Rev. B **42**, 587 (1990).
[11]P. Zeppenfeld, U. Becher, K. Kern, and G. Comsa, Phys. Rev. B **45**, 5179 (1992).
[12]C. Girard and C. Girardet, Surf. Sci. **195**, 173 (1988).
[13]M. Head-Gordon, J.C. Tully, C. Rettner, C.B. Mullins Mulins, and D.J. Auerbach, J. Chem. Phys. **94**, 1516 (1991).
[14]P. Zeppenfeld, U. Becher, K. Kern, R. David, and G. Comsa, Phys. Rev. B **41**, 8549 (1990).
[15]G. Xu, S.L. Bernasek, and J.C. Tully, J. Chem. Phys. **88**, 3376 (1988).
[16]J.C. Tully, Surf. Sci. **111**, 461 (1981).
[17]A.D. Novaco, Phys. Rev. B **19**, 6493 (1979); A.D. Novaco and J.P. McTague, Phys. Rev. Lett. **38**, 1286 (1977).
[18]C.R. Fuselier, J.C. Raich, and N.S. Gillis, Surf. Sci. **92**, 667 (1980).
[19]L.K. Moleko, B. Joos, T.M. Hakim, H.R. Glyde, and S.T. Chui, Phys. Rev. B **34**, 2815 (1986).
[20]C. Girardet and C. Girard, Surf. Sci. **201**, 278 (1988).
[21]C. Schwartz and R.J. Le Roy, Surf. Sci. **166**, L141 (1986).
[22]K. Kern, P. Zeppenfeld, R.L. Palmer, R. David, and G. Comsa, Phys. Rev. Lett. **57**, 3187 (1986).
[23]C. Ramseyer, C. Girardet, P. Zeppenfeld, J. Goerge, M. Büchel, and G. Comsa, Surf. Sci. (to be published).

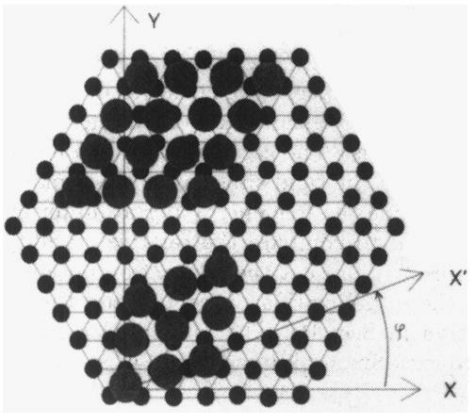

FIG. 1. Geometry of the Pt(111) substrate (dark small circles represent Pt atoms) with two adlayer HOC structures (hatched large circles represent Ar atoms). Lower: rotated (2×2) geometry, $m_1 = 2$ along $\mathbf{X}$ and $m_2 = 1$ along $\mathbf{Y}$; upper: nonrotated (4×4) geometry, $m_1 = 4$ along $\mathbf{X}$, and $m_2 = 0$ along $\mathbf{Y}$.